Furan fragmentation in the gas phase: new insights from statistical and molecular dynamics calculations

Ewa Erdmann[a], Marta Łabuda[a,*], Néstor F. Aguirre[b,c], Sergio Díaz-Tendero[c,d,e] and Manuel Alcamí[c,d,f,*]

[a] Faculty of Applied Physics and Mathematics, Gdańsk University of Technology, Narutowicza 11/12, 80-233 Gdańsk, Poland

[b,c] Los Alamos National Laboratory, Los Alamos, New Mexico 87545, USA

[c] Departamento de Química, Facultad de Ciencias, Módulo 13, Universidad Autónoma de Madrid, 28049 Madrid, Spain

[d] Institute for Advanced Research in Chemical Sciences (IAdChem), Universidad Autónoma de Madrid, 28049 Madrid, Spain.

[e] Condensed Matter Physics Center (IFIMAC), Universidad Autónoma de Madrid, 28049 Madrid, Spain.

[f] Instituto Madrileño de Estudios Avanzados en Nanociencias (IMDEA-Nanociencia),

28049 Madrid, Spain

ABSTRACT

We present a complete exploration of the different fragmentation mechanisms of furan (C_4H_4O) operating at low and high energies. Three different theoretical approaches are combined to determine the structure of all possible reaction intermediates, many of them not described in previous studies, and a large number of pathways involving three types of fundamental elementary mechanisms: isomerization, fragmentation and H/H_2 loss processes, this last one was not yet explored. Our results are compared with the existing experimental and theoretical investigations for furan fragmentation. At low energies the first processes to appear are isomerization, that always imply the breaking of one C-O bond and ones or several hydrogen transfers, at intermediate energies the fragmentation of the molecular skeleton becomes the most relevant mechanism and H/H_2 loss are the dominant processes at high energy, but the three mechanisms are active in very wide energy ranges and therefore at most energies there is a competition among them.

.

1. INTRODUCTION

Furan (C_4H_4O, see Scheme 1), is a five-membered heterocyclic ring molecule, which is one of the simplest constituents of several important biologically active macromolecules (biotin, vitamin B_{12}) [1]. It can be regarded as an analogue of the carbon ring (tetrahydrofuran molecule) of deoxyribose (dR) sugar, which is the backbone molecule in nucleic DNA acid. This simple aromatic compound and its derivatives are also components of conducting polymers[2] and play an important role in combustion chemistry, such as in the production of more ecological types of biofuels converted from solid biomass [3] [4] [5]. Also interestingly, furan is present in the commercial food industry, particularly in the nourishments which undergo heating processes [6]. In this respect, furan's toxicity and aspects of risk assessment of potential carcinogenic effects have been widely analyzed. For instances several studies have been performed to determine furan toxicity in coffee products [7] [8] [9]. However, in the current state of knowledge, the mechanisms of the carcinogenesis induced by human exposure to furan are not yet well established and therefore, there is still an interest in new studies to fully understand the decomposition of this heterocyclic compound under different conditions.

More recently, the interest in furan has been renewed due to the wide range of investigations of the radiation damage effects in biological systems. Since almost thirty years, significant effort is made in order to understand the mechanisms of genotoxic effects induced by the radiation in biological tissue. It has been shown that different types of irreversible damage are induced by crossing of the radiation tracks with DNA [10] [11] [12] [13] (and references therein). Molecular damage is the result of physical events: the deposition of energy and production of ionized and excited states of the molecules, or chemical events: production of radicals and other molecular products [14] [15]. From the chemical point of view, the most significant biological consequences are due to single- and double-strand breaks of DNA helix. The majority of these events are generated by secondary particles such as low-

3

energy electrons [16] [17] [18], radicals [13] and singly or multiply charged ions [14] [15] [19] which play a crucial role in structural and chemical modifications in DNA constituents. For this reason, theoretical and experimental investigations of the action of multiply charged ions on the building blocks of nucleic acids have raised great interest [14] [15] [19] [20] [21] [22] [23] [24] [25] [26] [27] [28]. From the theoretical point of view, the work of O. Mó and M. Yáñez, has been pioneer in the application of computational chemistry tools to study fragmentation of biomolecules [29] [30], as for instances the study of the unimolecular reactivity of the complexes of nucleobases (thymine or uracil), with metal ions (Co, Ca, Ni, Zn or Cu) [31] [32] [33]. Taking into account the importance of furan molecule from biological point of view, it seems that this simple molecule is very attractive to study, in collision with electrons [34] [35], ions [36] or synchrotron radiation [37] [38] [39] [40] [41] [42] [43]. Additionally, since our motivation to investigate this molecule is driven by its simplicity, it is also an ideal choice for the verification of the theoretical approaches used in our work.

The fragmentation of furan has been investigated extensively from both experimental [41] [43] [44] [45] [46] and theoretical [47] [48] [49] points of view. A first scheme for the thermal decomposition of furan molecule has been proposed by Lifshitz and co-workers[44], in the shock tube experiment, and more recently, by Fulle et al.[45] These studies of furan pyrolysis showed two possible unimolecular reaction channels occur directly from furan, namely: (1) $CH_3C{\equiv}CH$ + CO and (2) $HC{\equiv}CH$ + $H_2C=C=O$, and major decomposition products as methylacetylene (propyne) (C_3H_4), carbon monoxide (CO) and acetylene (HCCH) were identified. However, this study did not analyze the details of the decomposition processes and therefore, the mechanism of the formation of the various products was still unclear. Previous theoretical studies have proposed up to four different pathways for furan fragmentation in the ground state. The earliest theoretical investigation of unimolecular decomposition of furan by quantum chemistry methods was performed by Liu et al.[47] The unimolecular decomposition

4

channels of furan were determined by density functional theory and high-level *ab initio* calculations. The results obtained confirmed the two reaction pathways proposed by Lifshitz et al. [44]. The mechanisms proposed rely on the shift of hydrogen atoms (H_7 and H_8 position) followed by the opening of the ring by breaking $C_\alpha(1)$-O bond and then subsequent dissociation to give $CH_3C{\equiv}CH$ + CO fragments or followed by a concerted $C_\beta(2)$-$C_\beta(3)$ and O-$C_\alpha(4)$ bond cleavage to form $HC{\equiv}CH$ + $H_2C{=}C{=}O$. They also conclude that the formation of $CH_3C{\equiv}CH$ + CO is more likely to occur in the unimolecular dissociation of furan on the ground state potential energy surface (PES). Sorkhabi et al.[41] studied the dissociation dynamics of furan at 193 nm using photofragment translation spectroscopy technique with tunable vaccum ultraviolet (VUV) probe provided by intense synchrotron radiation. Three channels were observed, two in the agreement with the previous pyrolytic [44] [45] results and a third channel, namely (3) HCO + C_3H_3 not observed before. It was proposed, that the possible mechanism for this channel may occur by the opening of the ring via $C_\alpha(1)$-O bond cleavage on the electronically excited state, followed by 2,3 hydrogen shift and finally $C_\beta(3)$-$C_\alpha(4)$ bond breaking to obtain HCO + propargyl radical (C_3H_3).

Up to now, the most complete work on theoretical investigation of furan decomposition was presented by Sendt et al.[49]. These studies are based on an exploration of the PES by high level *ab initio* methods, at CASPT2, CASSCF and G2-MP2 levels of theory. They confirmed, that the most favoured unimolecular initiation of decomposition mechanisms occurs through the formation of α-carbene or β-carbene intermediates rather than biradical ring opening. The α-carbene fragments to $CH_2{=}C{=}O$ + $HC{\equiv}CH$ while the β-carbene isomerizes to formyl allene, $CH_2{=}C{=}CHCHO$, that can further evolve and fragment to $CO{+}CH_3C{\equiv}CH$ via concerted mechanism involving a 1,4 hydrogen transfer and a $C_\alpha(1)$-$C_\beta(2)$ bond fission or it can, with low probability, directly decompose to HCO + $HCCCH_2$. These results were also confirmed by Tian et al.[50] In their study of furan/oxygen/argon flames using tunable

synchrotron VUV photoionization and molecular-beam mass spectrometry and where they proposed a kinetic combustion model for furan, based on experiment as well as calculations using the CBS-QB3 method [51].

The nonadiabatic photoinduced ring opening occurring in the lowest excited singlet states of furan was investigated theoretically by Gromov et al. [52] by *ab initio* equation of motion coupled cluster singles and doubles method (EOM-CCSD)[53], and recently by using multiconfigurational time-dependent Hartree (MCTDH) wave-packet propagation techniques and an exploration of the PES[54] [55]. Also *ab initio* nonadiabatic dynamics have been used to reveal ultrafast deactivation from second excited state to ground state in Furan[56].

Despite all these efforts to understand the mechanisms of furan fragmentation further studies still remain necessary, especially regarding mechanisms different from direct unimolecular fragmentation of the furan C-C and C-O bonds, such as the loss of H or H_2, isomerizations linked to these H loss, or multifragmentation channels in which more than two bonds are broken. Our main aim in this work is not only to study these mechanisms, but also to establish a methodological protocol, based on different theoretical approaches, to provide complementary information on the decomposition processes of molecules under high energetic conditions. In this respect, by the detailed investigations of the processes in the furan decomposition, we are able to determine new structures and pathways which were not yet explored. Statistical methods applied here to explore further fragmentation steps allow to identify the most stable products particularly when more than two fragments are produced. Three methodologies are used with the objective to determine the most abundant fragmentation channels as well as nature of the mechanisms, and structure of the different fragments.

In the first step, our approach makes use of molecular dynamics (MD) simulations at different excitation energies of the system, which allows to obtain more reaction pathways by

6

purely statistical investigations. As an outcome of the simulation we can obtain a fragmentation "movie" showing how the products of the decomposition reaction are formed and scattered into space. This will yield to the observation of the direct (opening of the ring, bond breaking, migration of hydrogen atoms, isomerization) and time-delayed mechanisms (further decomposition of the products). A systematic analysis of molecular dynamics results, in the second step, will help to identify critical points such as minima and transition states on the PES schemes that cannot be easily obtained by using chemical intuition. By performing first MD simulations for different values of the excitation energy to the system we obtain the probability of evolving through the different channels, but also from the products obtained in these dynamics we can identify structures that can be considered as a starting point in the further exploration of the PES. At the third step, a newly developed statistical Microcanonical Metropolis Monte Carlo (M_3C) method is applied. It is worth to mention that this method has been recently [57] implemented for few exemplary applications and has never been applied to study complex molecules with several type of atoms and with a large number of possible isomers. From M_3C calculations we obtain the statistical distribution of all possible fragmentation channels as a function of the internal energy of the molecule in the limit where the system has infinite time to evolve. A great advantage of this method is the low cost of calculations in comparison to MD or exploration of the PES.

As we will show, combining two different techniques as MD and purely statistical method with PES exploration, has the advantage of creating a general picture of the mechanism of decomposition of furan covering low and high excitation energies. To the best of our knowledge, our present investigation, is the first theoretical work in which decomposition of furan molecule obtained by the different methodological scenarios is considered in such a complete way.

This article is organized as follows. In section 2, we present the theoretical methods and give technical details of the computational procedures used in our calculations. In section 3, we present, analyse and discuss our results with respect to the current state of knowledge and finally we provide conclusions and remarks.

2. COMPUTATIONAL DETAILS

In a first step, MD simulations were done in order to identify the most probable mechanisms and the structure of the potential final products. The *ab initio* atom-centered density matrix propagation (ADMP) method [58] [59] [60] with B3LYP functional and 6-31G(d,p) basis set has been employed to study the dynamics of neutral furan molecule. Propagation time of the simulations has been limited to t_{max}= 500 fs, which proved to be feasible for process under consideration. Time step of 0.1 fs and fictitious electron mass of 0.1 amu were chosen to ensure conservation of the total energy and good separation between electronic and nuclear degrees of freedom. Although the lifetime for reaction is expected to be much longer than 500 fs, our choice is proved to be sufficient to identify the most probable products of the decomposition of furan molecule and gives insight into the mechanism of fragmentation. That is also why the MD simulations are the initial steps in our approach and they have to be completed by the further exploration of the energy profiles of the PES for the observed processes. The excitation energy, varying from 5 eV to 30 eV in steps of 1 eV, was randomly distributed over all degrees of freedom of the molecule. Various initial velocities allow for conducting different simulations from the same starting structure, and thus performing statistical analysis over calculated 150 trajectories for each energy. A total of 3900 trajectories were run.

In order to gain complementary energetic and structural information of the fragmentation mechanism, we performed calculations of reactants, intermediates, transition states and products on the PES of neutral furan. Geometry optimizations and evaluations of the harmonic vibrational frequencies and Zero-point energy (ZPE) corrections were carried out with the density functional theory using B3LYP functional and initially a 6-311++G(d,p) basis set. Finally, at the same level of theory we performed intrinsic reaction coordinate (IRC) calculations to confirm whether obtained transition states indeed connect the right minima. In order to obtain more reliable results all structures were re-optimized with a larger, 6-311++G(3df,2p) basis set and frequencies and ZPE corrections were re-evaluated at this level.

All quantum chemistry calculations were carried out using Gaussian09 software [61].

Lastly, our final approach employed extended Microcanonical Metropolis Monte Carlo method (MMMC) as recently implemented in the M_3C code[57]. This statistical technique allowed us to study the fragmentation process of various systems by random sampling of accessible phase space until the maximum entropy region is reached. In order to perform M_3C simulation one needs to create a database of all possible fragments corresponding to different chemical formula, and for each of them different isomers can exist. M_3C interface with GAUSSIAN package allows performing stochastic isomer search for each fragment, by creating user-fixed number of trial geometries and subsequently optimizing them at lower level of theory (B3LYP/6-311G). This approach allowed to identify 44 possible fragments of furan (i.e. corresponding to 44 molecules of different chemical formulas). The automatic search of isomers led in total, to 226 different isomers for these fragments. In order to improve the obtained geometries we performed subsequent optimizations and vibrational frequencies calculations at higher level of theory (B3LYP/6-311++G(d,p)). After establishing the database with all possible fragments it is possible to perform the M3C calculation.

The reference molecule selected as the initial structure was the cyclic geometry of C4H4O (C4H4O.q0.m1-4, see SI). Simulation parameters were first tested until reaching the convergence. The final set of parameters used were: system radius of 13Å, Markov Chain sequence V, T, R, 5S:0, V, T, R, 5S:1:-1, (see Ref. 57 for explanation of the possible sequences and notation used for the Markov Chain) and 800 000 events for each one of the 50 numerical experiments performed. Excitation energy was scanned up to 20 eV with a step of 0.5 eV.

All structures presented in this work have been upload to the IoChem-BD database [62].

3. RESULTS AND DISCUSSION

3.1 Molecular Dynamics Simulations

Extensive statistical analysis of the trajectories obtained allows identifying the most abundant processes as a function of the excitation energy of the system. In Figure 1 we present the statistical analysis of the 3900 trajectories obtained in the MD simulations. We have characterized the different trajectories by the final structure obtained at the end of each simulation (500 fs) and assumed bonds to be broken when the distance between atoms exceeded R = 2.5 Å. The observed mechanisms can be divided into four groups: (1) isomerization, (2) isomerization + fragmentation of the carbon structure, a process that will be referred hereafter as skeleton fragmentation, (3) H/H$_2$ loss + isomerization and (4) H/H$_2$ loss + fragmentation.

Isomerization of the neutral furan molecule starts when excitation energy is above 9 eV and is the dominant process between 9 and 16 eV. As shown in Figure 2, where snapshots of the most significant trajectories are given, isomerization always implies the breaking of one C-O bond and the intramolecular transfer of one or several hydrogens. In none of the

10

trajectories the breaking of the C-C bond to form isomers with an ether group was observed, in agreement with previous calculations [47] [48] [49]. A deeper analysis of the MD trajectories is given in Figure 3 and allows having a more detailed view of the products obtained and their relative importance in the fragmentation of Furan. Figure 3a shows that mainly five isomeric forms, corresponding to the five snapshots for isomerization given in Figure 2, are obtained at the final step of the trajectories. The optimized structures and relative energy of these isomers are shown in Figure 4. The most probable one correspond to a formyl-allene structure ($H_2C=C=CH-CHO$, 3 and 4 in Figure 4 and snapshots a in Figure 2), followed by an isomer with an alkyne-alcohol structure, not considered in previous theoretical studies [47] [48] [49] ($HC\equiv C-CH-CHOH$, 5 and 6 in Figure 4 and snapshots b in Figure 2). The other isomeric structures correspond to the formation of a non-stable terminal carbene ($:CH-CH=CH-CHO$), that evolve to a cyclopropane substituted by a CHO group, (see 13 and 14 in Figure 4 and snapshots c in Figure 2) a mechanism neither considered before, a formyl-alkyne structure ($HC\equiv C-CH_2-CHO$, 7 and 8 in Figure 4 and snapshots d in Figure 2), and the formation of a terminal $-HC=C=O$ group ($H_2C=CH-CH=C=O$, 9 and 10 in Figure 4 and snapshots e in Figure 2). As shown in Figure 4 all these isomers are among the most stable ones and their relative energies with respect to Furan are less than 2 eV, and play a significant role in the decomposition of this molecule. Nevertheless, there is not a direct connection between their relative stability and their production yield shown in Figure 3. For instances, 9 and 10 are the second most stable structures after furan but, according to Figure 3, present the lowest yield of the five channels described. This is due to the presence of energy barriers in their mechanisms that will be discussed in detail in the next subsection.

Figures 1 and 3 also show that as the excitation energy increases above 16 eV the percentage of trajectories ending in one of these isomers decreases. This fact does not mean that the isomerization becomes less important, it just reflects that at higher energies

11

isomers appear earlier in the MD trajectories and at 500 fs they have already evolved towards fragmentation. Indeed, as we will discuss later, two other relevant isomers (1 and 2 in Figure 4) corresponding to carbene cyclic structures appear in the simulations, but they are very unstable and, in all trajectories obtained, they have evolved at 500 fs either toward fragmentation or toward one of the isomers described before.

The processes denoted as skeleton fragmentation involve the breaking of a C-C, after C-O breaking/isomerization and lead to the formation of two fragments (typically $CO+C_3H_4$ or $HCCH + H_2CCO$), but without further loosing H or H_2. As we can see in Figure 1a, isomerization and fragmentation start at similar energies around 10-11 eV, and between 17 and 23 eV skeleton fragmentation dominates. Snapshots of typical trajectories are shown in Figure 2. More quantitative results are given in Figure 3b, which shows the channels leading to two fragments as a function of the excitation energy. The channel that appeared first in the dynamical simulations, and is also the most abundant at nearly all energies is the fragmentation into acetylene (HCCH) and ethenone (H_2CCO). The highest probability of obtaining these fragments occurs for the energy of 18 eV. Second most populated channel for two-fragment dissociation is production of CO and C_3H_4 with highest probability of occurrence for an excitation energy of 17 eV. The fragment C_3H_4 was observed in three different structural forms: H_2CCCH_2 (allene), H_3CCCH (propyne) or H_2CCHCH (cyclopropene). The total numbers of trajectories in which these isomers appear are 96, 44 and 35, respectively. As we will show later the order of appearance agrees with their relative stability.

The loss of atomic and molecular hydrogen followed by isomerization starts at an energy of 13 eV and reaches maximum probability at 24 eV and 21 eV, respectively (see Figure 3b), this is in agreement with previous studies that pointed out that C–H bond dissociation energy

in furan is exceptionally high because of the thermodynamic instability of the produced radical[63,64]. Sendt et al. [49] reported unusually high C–H bond enthalpies of 506.3 and 513.6 kJ mol-1 (calculated from the isodesmic reaction: $C_4H_4O + CH_3 \rightarrow C_4H_3O + CH_4$ for H_α and H_β, respectively) and dismissed unimolecular C–H bond fission in the temperature range of 1100-1700 K. Our dynamical simulations show a competition between H_α and H_β loss, being the former slightly more frequent: 91 vs 73 trajectories. This family of trajectories starts with the loss of H or H_2 and are followed by an isomerization of the remaining H_3C_4O or H_2C_4O fragment. The structure of the different isomers produced in these processes will be discussed in the next section.

Finally, the loss of H or H_2 can be followed by a further fragmentation of the C-O and C-C bonds. These processes require more excitation energy in the molecule; they start at 14 eV, and with increasing energy, i.e. energies larger than 22 eV, multifragmentation (production of more than two fragments) becomes the dominant process (see Figure 1b and 3c). Figure 2 shows snapshots of the most relevant trajectories for these processes, and consist of initial H or H_2 loss and subsequent fragmentation. Channel producing H_2C_3, CO and H_2 is the dominant and is one of the most relevant channels when all energies and processes are considered. This channel appears first at the internal energy of 14 eV and its occurrence reaches the highest value at 28 eV. The most important channels of H loss occur after the channel of H_2 loss, at 15 eV ($CO/H_3C_3/H$) and later at 20 eV ($HC_2O/H_2C_2/H$). As in the case of H loss + isomerization channels, the majority of single hydrogen elimination occurs from alpha position.

Looking at the global picture obtained from the MD simulations several, non-trivial results can be stressed: although, as expected, multifragmentation channels dominate at high energies it is relevant to note that dissociation in two fragments, either skeleton

13

fragmentations or H/H$_2$ loss, are still key processes at high energy and even isomerization without fragmentation is observed up to energies close to 25 eV. Previous theoretical studies [47] [48] [49] have focused on the mechanisms of isomerization ending in the fragmentation into two large fragments, but H/H$_2$ loss and multifragmentation have not been previously studied and they represent important channels under high energetic conditions but also at intermediate energies. Regarding mechanisms starting with H/H$_2$ loss subsequent fragmentation of the remaining fragment dominates over isomerization for most of the energy ranges in which these processes appear (see Figure 1a).

3.2 Exploration of the Potential Energy Surface

In order to provide complementary information on the isomerization/fragmentation mechanisms and extend the possible outcomes of the dynamical simulations we have performed exploration of the PES of neutral furan. Following a similar scheme than in the MD simulations, we will discuss first the process just leading to isomerization of the system previous to fragmentation and in the following subsections we will analyse the skeleton fragmentation and H or H$_2$ loss. Several authors have explored the PES for isomerization/fragmentation of furan, the two most systematic ones have been performed by Liu et al. [47] [48] and by Sendt et al. [49], but they have restricted their exploration of the PES to isomerization and fragmentation of the molecular skeleton in two large fragments.

Isomerization processes: Figure 4 gives the structures of all isomers obtained as minima in our exploration of the PES. We have based this exploration mainly on the analysis of the trajectories of the MD simulations. As it can be seen in Figure 4, this strategy allowed us to locate more minima than previously studied, indeed 9 out of the 18 structures depicted in Figure 4 were not studied before including some of the most stable ones, as 9, 10 or 18.

In the analysis of the isomerization processes we have also located all the Transition States connecting the minima in Figure 4. Their structures are given in Figure 5 and a schematic representation of the reactions paths connecting all isomers included in Figure 4 is given in Figure 6. In figures 4 and 5 relative energies using the 6-311+G(d,p) and 6-311++G(3df,2p) basis sets are compared. As can be seen differences in relative energies are always lower than 0.5 eV, all the structures obtained at both level of theory are given in the SI. In the rest of the section all the discussion will refer to the B3LYP/6-311++G(3df,2p) results. In agreement with previous work, from Furan the two reaction paths showing the lowest energy barriers (indicated as *p1* and *p2* in Figure 6) imply 1,2 or 2,1 hydrogen transfers to form cyclic carbenes, in which the carbene atom can be in C_α or C_β positions, structures 1 and 2 respectively. Structure 1 can only evolve towards fragmentation (see next subsection) while structure 2 can further evolve to formyl-allene (3 and 4). The low energy barrier associated with this path is consistent with the fact that isomers 3 and 4 are obtained in a larger number of trajectories. Nevertheless, it has to be kept in mind that the number of trajectories in the MD simulations for a particular channel do not necessarily correlates with the barrier heights of the corresponding TS, due to the possibility of non-statistical dynamics, especially at high excitations energies. From these structures an H transfer from $C_\alpha(4)$ to O is done through TS3-5 that is located just 2.66 eV above furan and leads to alkyne-alcohol structures 5 and 6, which represents the second most probable channel according to the MD simulations. Alternatively, a 1,3 H transfer also involves a low energy barrier (TS4-9) and leads to the formation of the very stable isomers 9 and 10. Two other possible isomerization processes (*p3* and *p4* in Figure 6) leads to higher energy barrier around 3.5 eV and consistently a lower number of trajectories are obtained for these channels, 36 and 67, respectively. It has to be mentioned that, as discussed by Sendt et al.[49] structure may present a biradical character. Our calculations of the corresponding triplet states of 13 and 14 isomers using an unrestricted

15

DFT formalism reveal that their relative energy with respect furan are 2.98 and 2.93 eV respectively, and the interconversion barrier TS13-14 located at 3.38 eV. Fragmentation into $CO + CHCHCH_2$ implies a barrier located at 3.23 eV with respect neutral furan. All these results show that the biradical mechanism for ring opening is less favourable in agreement with the conclusions of Sendt et al. .[49] The last possible isomerization processes *p5* lead to very unstable 15 and 16 structures and no trajectories in the MD simulations were predicted to follow this reaction path.

Skeleton fragmentation: As shown in Figure 7a, direct fragmentation can be envisaged from structures 1, 3/4, 7/8 and 12. These mechanisms have been already described in previous studies [47] [48] [49]. The most direct fragmentation mechanism from Furan is the 1,2 H transfer to give structure 1 and from there two fragmentations are possible. $HCCH + H_2CCO$, which is the one that presents the lowest energy barrier (3.55 eV above Furan), while TS leading to fragmentation into $CH_3CCH + CO$ from 1 is 0.85 eV higher in energy. An alternative pathway to $CH_3CCH + CO$ with a slightly lower energy barrier is through isomerization to structure 7 before fragmentation. Two other mechanisms that can explain the loss of CO imply several isomerization steps ($2 \Rightarrow 3/4 \Rightarrow 9/10 \Rightarrow 12$), the energy barriers involved in these steps are 3.03, 3.14 and 3.21 eV respectively (see Figures 6 and 7) which are below the barriers required for fragmentation from 1 and 7. In this mechanism CO can be obtained directly from 4, but through an energy barrier located at 4.16 eV, or from 12 a process that presents the lowest TS for dissociation (3.21 eV).

A different fragmentation mechanism not described before is given in Figure 7b and proceeds first from isomerization to structure 13, which already requires overcoming a barrier of 3.52 eV. From this structure two different mechanisms lead to the fragmentation to CO

16

and C_3H_4 in cyclic forms (cyclopropene or cyclopropylidene). The former is more stable, but requires to overcome a larger energy barrier.

As discussed before, in the MD simulations C_3H_4 fragment was obtained in three isomeric forms. The PES obtained is consistent with the MD results in the sense that these three different isomers can be obtained in few steps. The lowest energy path would lead to the formation of CH_3CCH isomer, which needs to overcome a barrier located at 3.21 eV, to get H_2CCCH_2 the reaction path goes through a barrier located at 4.16 eV and cyclopropene is obtained after crossing a barrier of 5.51 eV. And extra isomer, cyclopropylidene, can be obtained after several steps, the highest one located at 4.52 eV. Their stability follows a different order being H_2CCCH_2 the most stable one (0.95 eV), followed by CH_3CCH (1.05 eV), cyclopropene (2.09 eV) and cyclopropylidene (3.95 eV). The MD simulation predicted that H_2CCCH_2 is the one obtained in more trajectories (96) followed by H_3CCCH (44) and cyclopropene (35), cyclopropylidene was not obtained in any trajectory. It has to be taken into account that in some of the MD simulations the internal energy considered was high enough to overcome these barriers and, in these cases, the statistical distribution of final products should be the main effect that prevails over the differences in energy barriers.

H and H₂ fragmentation: First process that we can observe is H loss and subsequent isomerization. As stated before, our dynamical simulations of highly excited furan show a competition between $H\alpha$ and $H\beta$ loss, with a small preference toward alpha position (52% and 48% of all trajectories including H loss, respectively). The computed PES (see Figure 8) shows that the hydrogen elimination from both positions proceeds without energy barrier and are of equal height (5.07 eV). Resulting C_α-furyl and C_β-furyl structures (23 and 19) present practically unchanged geometry to that of furan. The maximum variation observed in geometrical parameters appeared after $H\alpha$ loss and led to decrease of $C_\alpha(4)$-O bond length by

17

0.03 Å as well as decrease in C_α-C_β-C_β angle and increase in O-C_α-C_β angle by approx. 3°. As already described in [49] the single electron of these radicals occupies a π type orbital and our analysis of the spin densities shows that the unpaired electron is located on the carbons that lost the hydrogen. As shown in Figure 8, further isomerization after H loss goes through cleavage of the $C_\alpha(4)$-O bond of the C_α-furyl or $C_\alpha(1)$-O of the C_β-furyl concerted with H transfer to the carbon from which hydrogen was previously removed, leading to structures 24 and 20. Structure 24 is favoured by both the final stability and the energy barrier involved, but its fragmentation is through a very large energy barrier of 8 eV. Alternatively from 20 we can observe direct fragmentation into HCCH + HCCO or subsequent isomerization from structure 20 by H transfer from $C_\beta(2)$ to outer carbon $C_\alpha(1)$ giving structure 21 and rotation of the dihedral angle O-C_α-C_β-C_β leading to structure 22. From this structure fragmentation into CO + CH_2CCH involves a very low energy barrier of just 0.65 eV. As mentioned before, from 24 a direct fragmentation would lead to the same products but crossing a very high energy barrier.

In summary, loss of H would imply a first step of 5 eV from which barriers located at around 7-8 eV can lead to further loss of CO. These processes are located at higher energy to those discussed above for isomerization or skeleton fragmentation, explaining why they only appear in the dynamics at high energies.

Direct loss of H_2 are also obtained in the MD simulations. The corresponding PES are shown in Figures 9 and 10. Different reaction paths are observed depending on the origin of the two emitted hydrogens. In our dynamical studies we notice significant prevalence of H_2 loss from alpha and beta positions of one side of the furan ring. The frequency of H_2 loss in a decreasing order is: adjacent H_α and H_β (62%) > two H_α (16%) > opposite H_α and H_β (13%) > two H_β (9%).

18

The PESs studied correspond to these possibilities of H_2 loss. For the emission from adjacent H_α and H_β positions pathways start from structures 1 and 2 where H presents a better spatial distribution for emission of H_2. Barriers for H_2 loss from β-carbene (2) or α-carbene (1) are very similar (6.17 and 6.30 eV, respectively) and both lead to structure 25. From there, subsequent ring opening can give structure 26 that further fragments in CO + Cyclic C_3H_2.

A slightly lower H_2 barrier is obtained when hydrogens are emitted from two H_β positions (see Figure 10), in this case the first step is a 2,3 H transfer leading to structure 7, in which the furan cycle is opened, emission of H_2 is obtained after crossing a barrier of 5.86 eV (higher than the one reported before of 4.30 eV for skeleton breaking from 7). Loss of H_2 implies the formation again of a cyclic structure, 27, that can further evolve through isomers 28, 29 and 30 and eventually fragment in CO + Cyclic C_3H_2 as in the previous channels.

Loss of H_2 from two H_α or H_α and H_β from opposite sides of the furan ring, follow a common mechanism also presented in Figure 10. The first step is the formation of structure 2, from there H can be extracted from the two alpha positions. As the hydrogens in position 1 were originally in Furan in alpha or beta positions, the mechanism can be interpreted as either two H_α or H_α and H_β loss from opposite sides. This mechanism presents the highest energy barrier (7.23 eV). Further stabilization of the system can additionally occur after ring opening to structure 32, common to the previously described mechanism.

Globally, the H_2 loss from two beta positions should be the most favourable-channel for H_2 emission. The low occurrence of this channel in the dynamical simulations can be explained by deterring properties of stable structure 7 before the transition state, in this case the ring opens in structure 7 and have to close again to give structure 27, while in the others paths of

19

H$_2$ loss the ring structure is kept when going from 1 or 2 towards 25 or 31 and once these structures are formed they evolve through a low energy barrier to other stable isomers.

Compared with H loss, initial H$_2$ emission presents higher energy barriers (in the range 5.86 - 6.30 eV vs 5.07 eV) but isomerization and further fragmentation imply similar energies in both cases. Final fragments are more stable in the case of H$_2$ loss (4.10 eV vs 4.76 eV or 6.31 eV). The relative energies of the final products are coherent with the MD results of Figure 3b, where the most abundant channel found was C$_3$H$_2$ + CO + H$_2$ and the most important channels of H loss occur after the channel of H$_2$ loss, at 15 eV (CO/H$_3$C$_3$/H) and later at 20 eV (HC$_2$O/H$_2$C$_2$/H).

3.3 Microcanonical Metropolis Monte Carlo (M$_3$C) calculations

M$_3$C calculations offer a complementary viewpoint; In this methodology a statistical distribution of all possible fragmentation channels is obtained. We consider the limit where the energy of the system is enough to overcome all energy barriers (i.e. only final minima in the potential energy surface are taken) and the system has infinite time to evolve (within the ergodic hypothesis). All possible species and fragments are included, even they are not easily accessible in the PES (disregarding barriers), and their final distribution is obtained taking into account the relative energies of all fragmentation channels and, most importantly, their density of states (rotational, vibrational... see Ref. 57 for details). Notice that in the M$_3$C simulations, the excitation energy is not comparable with the one in the molecular dynamics due to the different timescale: while the MD simulations run up to 500 fs and only the very first steps of the fragmentation are considered, in the M$_3$C infinite time limit is assumed and complete redistribution of the excitation energy over all fragments.

In the M$_3$C simulation we have considered all possible relevant fragments that are minima of the PES. Table 1 summarizes them: in total 226 isomers corresponding to 44 different

chemical formulas have been included in the dataset for the M_3C simulations. The geometries of all these species are given in the Supporting Information.

Figure 11 presents the results obtained with the M_3C calculations. The final distribution of the fragmentation channels and the molecular species in the excitation energy range considered is shown. We observe that the first channel CO/H_4C_3 appears at 1 eV. It can be noticed that with the increase of excitation energy up to 4.5 eV, it is the only fragmentation channel with probability of 100%. The situation changes after reaching 5 eV, when a second channel H_2C_2/H_2C_2O appears and gets a maximum probability of 30% at 6.5 eV. Both channels are also dominant in the AIMD simulations at intermediate energies, but the second one H_2C_2/H_2C_2O presents higher probability in all the energy range. This difference points that at longer simulation times we would expect an enhance probability of the CO/H_4C_3 channel in the AIMD simulations. The high stability of the CO fragment is responsible for the high probability of channels with this fragment in the M_3C results. This is coherent with the fact that the exit channels in the PES are more stable when CO is produced (see in figure 7 channels $H_2CCCH_2 + CO$ and $CH_3CCH + CO$ in comparison with channels $HCCH + H_2CCO$). All these results are in good agreement with the experimental measurements of furan pyrolysis (Refs 44 and 45), where they show that these two channels are the dominant ones.

The three-fragments channel observed at lower excitation energy is $CO/H_2C_3/H_2$, it dominates in the excitation energy range from ~ 6 eV to ~11 eV with a maximum at 8.5 eV. At higher energies we can also notice four- and five-fragments channels involving either atomic and molecular hydrogen loss being the dominant ones $CO/HC_3/H_2/H$, $CO/C_3/H_2/H_2$, and $CO/C_3/H_2/H/H$. These channels, although highly stable and entropically dominant, as reflected in the M_3C results, do not appear in the AIMD simulations since we do not allow

21

the system to evolve long enough to be observed. They were not considered in our previous discussion of the PES since they present high-energy barriers (at least of ~10 eV).

A summary with the observed channels in the M_3C simulations is given in scheme 2. The general trend shows that channels with CO dominate at low energies; channels with loss of atomic and/or molecular hydrogen follow decarboxylation. In the molecular skeleton cleavage, the presence of species with three carbon atoms, C_3H_X ($X = 0–4$) is also observed. On the contrary, as we present above, in the dynamics the loss of H or H_2 also appear at intermediate excitation energy when part of the internal energy is sufficient to break the C-H bond.

4. CONCLUSIONS

The theoretical investigation of the fragmentation processes of furan molecule by combining three different theoretical methods allows to have a complete overview of the different fragmentation mechanisms operating at a wide range of energies. Molecular dynamics simulations allow to determine the range in which different processes dominates and identify several important intermediates, difficult to envisage just using chemical intuition, and that were not considered in previous works. At low energies the first processes to appear are isomerization, that always imply the breaking of one C-O bond and ones or several hydrogen transfers. Even though isomerization has been study before using different theoretical methods our computational strategy has allowed us to locate more minima than previously studied, indeed 9 out of the 18 structures found were not studied before including some of the most stable ones. A large number of pathways were explored to have a complete overview of the different fragmentation mechanism as the breaking of the carbon skeleton but also H/H_2 loss processes, that up to now were not yet explored despite the fact that at large energies H/H_2 loss are the dominant mechanisms. Our obtained results were compared with

22

the existing experimental and theoretical investigations of furan pyrolysis. Multifragmentation processes are difficult to study since they only appear at very long simulation time in the MD calculations or need to explore many potential isomer fragments. Statistical methods applied here allow to identify, at a small computational cost, all the possible isomer obtained in the fragmentation, 226 in the case of furan, and the most stable relevant multifragmentation channels.

ASSOCIATED CONTENT

All the structures obtained for the stable compounds and transition states presented in this work can be downloaded from the IoChemBD platform using the following link: https://iochem.ccc.uam.es/browse/review-collection/100/501/b4cb55022277e8f978925770

ACKNOWLEDGMENTS

REFERENCES

(1) Kappe, C. O.; Murphree, S. S.; Padwa, A. Synthetic Applications of Furan Diels-Alder Chemistry. *Tetrahedron*, **1997**, 14179–14233.

(2) Glenis, S.; Benz, M.; LeGoff, E.; Schindler, J. L.; Kannewurf, C. R.; Kanatzidis, M. G. Polyfuran: A New Synthetic Approach and Electronic Properties. *J. Am. Chem. Soc.* **1993**, *115* (26), 12519–12525.

(3) Román-Leshkov, Y.; Barrett, C. J.; Liu, Z. Y.; Dumesic, J. A. Production of Dimethylfuran for Liquid Fuels from Biomass-Derived Carbohydrates. *Nature* **2007**, *447*, 982-985.

(4) Mascal, M.; Nikitin, E. B. Direct, High-Yield Conversion of Cellulose into Biofuel. *Angew. Chemie - Int. Ed.* **2008**, *47* (41), 7924–7926.

(5) Tran, L. S.; Sirjean, B.; Glaude, P.; Fournet, R.; Battin-Leclerc, F.; Progress in detailed kinetic modeling of the combustion of oxygenated components of biofuels. *Energy (Oxf)* **2012**, *43* (1), 1–32.

(6) Crews, C.; Castle, L. A Review of the Occurrence, Formation and Analysis of Furan in Heat-Processed Foods. *Trends Food Sci. Technol.* **2007**, *18* (7), 365–372.

(7) Moro, S.; Chipman, J. K.; Wegener, J.-W.; Hamberger, C.; Dekant, W.; Mally, A. Furan in Heat-Treated Foods: Formation, Exposure, Toxicity, and Aspects of Risk Assessment. *Mol. Nutr. Food Res.* **2012**, *56* (8), 1197–1211.

(8) Waizenegger, J.; Winkler, G.; Kuballa, T.; Ruge, W.; Kersting, M.; Alexy, U.; Lachenmeier, D. W. Analysis and Risk Assessment of Furan in Coffee Products Targeted to Adolescents. *Food Addit. Contam. Part A* **2012**, *29* (1), 19–28.

(9) Guenther, H. Furan in Coffee. In *Coffee: Emerging Health Effects and Disease Prevention*; **2012**, 307–318.

(10) von Sonntag, C. *The Chemical Basis for Radiation Biology*; Taylor and Francis; 1st edition, 1987.

(11) Hill, M. A. Radiation Damage To Dna: The Importance of Track Structure. *PERGAMON Radiat. Meas.* **1999**, *31*, 15–23.

(12) Ward, J. Ionizing Radiation Damage to DNA, A Challenge to Repair Systems. *Advances in DNA Damage and Repair*. **1999**, 431–439.

(13) von Sonntag, C. *Free-Radical-Induced DNA Damage and Its Repair*; Springer-Verlag Berlin Heidelberg, **2006**.

(14) Schlathölter, T.; Hoekstra, R.; Morgenstern, R. Charge Driven Fragmentation of Biologically Relevant Molecules. *Int. J. Mass Spectrom.* **2004**, *233,* 1–3.

(15) Schlathölter, T.; Alvarado, F.; Bari, S.; Hoekstra, R. Ion-Induced Ionization and Fragmentation of DNA Building Blocks. *Phys. Scr.* **2006**, *73* (4) , C113-C117.

(16) Boudaïffa, B.; Cloutier, P.; Hunting, D.; Huels, M. A.; Sanche, L. Resonant Formation of DNA Strand Breaks by Low-Energy (3 to 20 eV) Electrons. *Science.* **2000**, *287*, 1658-1660.

(17) Huels, M. A.; Hahndorf, I.; Illenberger, E.; Sanche, L. Resonant Dissociation of DNA Bases by Subionization Electrons. *J. Chem. Phys.* **1998**, *108* (4), 1309-1312.

(18) Michael, B. D.; O'Neill, P. A Sting in the Tail of Electron Tracks. *Science.* **2000**, *287*, 1303-1304.

(19) Bacchus-Montabonel, M. C.; Łabuda, M.; Tergiman, Y. S.; Sienkiewicz, J. E. Theoretical Treatment of Charge-Transfer Processes Induced by Collision of C^{q+} Ions with Uracil. *Phys. Rev. A - At. Mol. Opt. Phys.* **2005**, *72* (5) 052706.

(20) Erdmann, E.; Bacchus-Montabonel, M.-C.; Łabuda, M. Modelling Charge Transfer Processes in C^{2+}- tetrahydrofuran Collision for Ion-Induced Radiation Damage in DNA Building Blocks. *Phys. Chem. Chem. Phys.* **2017**, *19* (30), 19722–19732.

(21) Erdmann, E.; Łabuda, M.; Díaz-Tendero, S.; Aguirre, N. F.; Alcamí, M. Charge Dependence of Fragmentation Process Induced by Ion Collisions with Furan Molecule. *J. Phys. Conf. Ser.* **2017**, *875*, 102021.

(22) Erdmann, E.; Łabuda, M. Electron Transfer Induced by Collision of Low-Energy Doubly Charged Carbon Ions with Tetrahydrofuran. *J. Phys. Conf. Ser.* **2015**, *635* (2), 22097.

(23) Agnihotri, A. N.; Kasthurirangan, S.; Nandi, S.; Kumar, A.; Galassi, M. E.; Rivarola, R. D.; Fojón, O.; Champion, C.; Hanssen, J.; Lekadir, H. Ionization of Uracil in Collisions with Highly Charged Carbon and Oxygen Ions of Energy 100 keV to 78 MeV. *Phys. Rev. A - At. Mol. Opt. Phys.* **2012**, *85* (3), 1–5.

(24) Capron, M.; Diaz-Tendero, S.; Maclot, S.; Domaracka, A.; Lattouf, E.; Lawicki, A.; Maisonny, R.; Chesnel, J.-Y.; Mery, A.; Poully, J.-C.; Rangama, J; Adoui, L; Martín, F; Alcamí, M; Rousseau, P; Huber, B. A. A Multicoincidence Study of Fragmentation Dynamics in Collision of γ-Aminobutyric Acid with Low-Energy Ions. *Chem.Eur. J.* **2012**, *18*, 9321.

(25) González-Magaña, O.; Tiemens, M.; Reitsma, G.; Boschman, L.; Door, M.; Bari, S.; Lahaie, P. O.; Wagner, J. R.; Huels, M. A.; Hoekstra, R.; Schlathölter, T Fragmentation of Protonated Oligonucleotides by Energetic Photons and C^{q+} Ions. *Phys. Rev. A - At. Mol. Opt. Phys.* **2013**, *87* (3), 1–13.

(26) Champion, C.; Lekadir, H.; Galassi, M. E.; Fojón, O.; Rivarola, R. D.; Hanssen, J. Theoretical Predictions for Ionization Cross Sections of DNA Nucleobases Impacted by Light Ions. *Phys. Med. Biol.* **2010**, *55* (20), 6053–6067.

(27) Bacchus-Montabonel, M.-C. Looking at Radiation Damage on Prebiotic Building Blocks. *J. Phys. Chem. A* **2013**, *117* (51), 14169–14175.

(28) Domaracka, A.; Capron, M.; Maclot, S.; Chesnel, J.-Y.; Méry, A.; Poully, J.-C.; Rangama, J.; Adoui, L.; Rousseau, P.; Huber, B. A. Ion Interaction with Biomolecular Systems and the Effect of the Environment. *J. Phys. Conf. Ser.* **2012**, *373*, 12005.

(29) Alcamí, M.; Mó, O.; Váñez, M. Computational Chemistry: A Useful (Sometimes Mandatory) Tool in Mass Spectrometry Studies. *Mass Spectrom. Rev.* **2001**, *20* (4), 195–245.

(30) Martín-Sómer, A.; Yáñez, M.; Gaigeot, M. P.; Spezia, R. Unimolecular Fragmentation Induced by Low-Energy Collision: Statistically or Dynamically Driven? *J. Phys. Chem. A* **2014**, *118* (46), 10882–10893.

(31) Rincón, E.; Yáñez, M.; Toro-Labbé, A.; Mó, O. Effect of Ni(ii), Cu(ii) and Zn(ii) Association on the Keto-Enol Tautomerism of Thymine in the Gas Phase. *Phys. Chem. Chem. Phys.* **2007**, *9* (20), 2531–2537.

(32) Hurtado, M.; Mó, O.; Yáñez, M.; Herrera, B.; Lamsabhi, A. M. New Insights into the Gas-Phase Unimolecular Fragmentations of [Cysteine-Ca]$^{2+}$ Complexes. *Comput. Theor. Chem.* **2014**, *1047* (1), 38–46.

(33) Lamsabhi, A. M.; Alcamí, M.; Mó, O.; Yáñez, M.; Tortajada, J. Gas-Phase Deprotonation of Uracil−Cu^{2+} and Thiouracil−Cu^{2+} Complexes. *J. Phys. Chem. A* **2006**, *110* (5), 1943–1950.

(34) Dampc, M.; Zubek, M. Dissociation and Fragmentation of Furan by Electron Impact. *Int. J. Mass Spectrom.* **2008**, *277* (1–3), 52–56.

(35) Dampc, M.; Linert, I.; Zubek, M. Ionization and Fragmentation of Furan Molecules by Electron Collisions. *J. Phys. B At. Mol. Opt. Phys.* **2015**, *48* (16), 165202.

(36) Wasowicz, T. J.; Pranszke, B. Interactions of Protons with Furan Molecules Studied by Collision-Induced Emission Spectroscopy at the Incident Energy Range of 50–1000 eV. *Eur. Phys. J. D* **2016**, *70* (8), 175.

(37) Tokaryk, D. W.; Culligan, S. D.; Billinghurst, B. E.; Van Wijngaarden, J. A. Synchrotron-Based Far-Infrared Spectroscopy of Furan: Rotational Analysis of the ν_{14}, ν_{11}, ν_{18} and ν_{19} Vibrational Levels. *J. Mol. Spectrosc.* **2011**, *270* (1), 56–60.

(38) Rennie, E. E.; Hergenhahn, U.; Kugeler, O.; Rüdel, A.; Marburger, S.; Bradshaw, A. M. A Core-Level Photoionization Study of Furan. *J. Chem. Phys.* **2002**, *117* (14), 6524–6532.

(39) Rennie, E. E.; Cooper, L.; Johnson, C. A. F.; Parker, J. E.; Mackie, R. A.; Shpinkova, L. G.; Holland, D. M. P.; Shaw, D. A.; Hayes, M. A. A Study of the Unimolecular Decomposition of Internal-Energy-Selected Furan Molecular Ions by Threshold-Photoelectron-Photoion Coincidence Spectroscopy. *Chem. Phys.* **2001**, *263* (1), 149–165.

(40) Pešić, Z. D.; Rolles, D.; Dumitriu, I.; Berrah, N. Fragmentation Dynamics of Gas-Phase Furan Following K-Shell Ionization. *Phys. Rev. A - At. Mol. Opt. Phys.* **2010**, *82* (1), 1–9.

(41) Sorkhabi, O.; Qi, F.; Rizvi, A. H.; Suits, A. G. Ultraviolet Photodissociation of Furan Probed by Tunable Synchrotron Radiation. *J. Chem. Phys.* **1999**, *111* (1), 100–107.

(42) Palmer, M. H.; Walker, I. C.; Ballard, C. C.; Guest, M. F. The Electronic States of Furan Studied by VUV Absorption, near-Threshold Electron Energy-Loss Spectroscopy and Ab Initio Multi-Reference Configuration Interaction Calculations. *Chem. Phys.* **1995**, *192* (2), 111–125.

(43) Urness, K. N.; Guan, Q.; Golan, A.; Daily, J. W.; Nimlos, M. R.; Stanton, J. F.; Ahmed, M.; Ellison, G. B. Pyrolysis of Furan in a Microreactor. *J. Chem. Phys.* **2013**, *139* (12), 124305.

(44) Lifshitz, A.; Bidani, M.; Bidani, S. Thermal Reactions of Cyclic Ethers at High Temperatures. III. Pyrolysis of Furan behind Reflected Shocks. *J. Phys. Chem.* **1986**, *90* (21), 5373–5377.

(45) Fulle, D.; Dib, A.; Kiefer, J. H.; Zhang, Q.; Yao, J.; Kern, R. D. Pyrolysis of Furan at Low Pressures: Vibrational Relaxation, Unimolecular Dissociation, and Incubation Times. *J. Phys. Chem. A* **1998**, *102* (38), 7480–7486.

(46) Vasiliou, A.; Nimlos, M. R.; Daily, J. W.; Ellison, G. B. Thermal Decomposition of Furan Generates Propargyl Radicals. *J. Phys. Chem. A* **2009**, *113* (30), 8540–8547.

(47) Liu, R.; Zhou, X.; Zhai, L. Theoretical Investigation of Unimolecular Decomposition Channels of furan4. *J. Comput. Chem.* **1998**, *19* (2), 240–249.

(48) Liu, R.; Zhou, X.; Zuo, T. The Pyrolysis Mechanism of Furan Revisited. *Chem. Phys. Lett.* **2000**, *325* (4), 457–464.

(49) Sendt, K.; Bacskay, G. B.; Mackie, J. C. Pyrolysis of Furan: Ab Initio Quantum Chemical and Kinetic Modeling Studies. *J. Phys. Chem. A* **2000**, *104* (9), 1861–1875.

(50) Tian, Z.; Yuan, T.; Fournet, R.; Glaude, P. A.; Sirjean, B.; Battin-Leclerc, F.; Zhang, K.; Qi, F. An Experimental and Kinetic Investigation of Premixed Furan/oxygen/argon Flames. *Combust. Flame* **2011**, *158* (4), 756–773.

(51) Montgomery, J. A.; Frisch, M. J.; Ochterski, J. W.; Petersson, G. A. A Complete Basis Set Model Chemistry. VI. Use of Density Functional Geometries and Frequencies. *J. Chem. Phys.* **1999**, *110* (6), 2822–2827.

(52) Gromov, E. V.; Trofimov, A. B.; Vitkovskaya, N. M.; Schirmer, J.; Köppel, H. Theoretical Study of the Low-Lying Excited Singlet States of Furan. *J. Chem. Phys.* **2003**, *119* (2), 737.

(53) Stanton, J. F.; Bartlett, R. J. The Equation of Motion Coupled-Cluster Method. A Systematic Biorthogonal Approach to Molecular Excitation Energies, Transition Probabilities, and Excited State Properties. *J. Chem. Phys.* **1993**, *98*, 7029.

(54) Gromov, E. V.; Trofimov, A. B.; Gatti, F.; Köppel, H. Theoretical Study of Photoinduced Ring-Opening in Furan. *J. Chem. Phys.* **2010**, *133* (16), 164309.

(55) Gromov, E. V; Lévêque, C.; Gatti, F.; Burghardt, I.; Köppel, H. Ab Initio Quantum Dynamical Study of Photoinduced Ring Opening in Furan. *J. Chem. Phys.* **2011**, *135* (16), 164305.

(56) Fuji, T.; Suzuki, Y. I.; Horio, T.; Suzuki, T.; Mitrić, R.; Werner, U.; Bonačić-Koutecký, V. Ultrafast Photodynamics of Furan. *J. Chem. Phys.* **2010**, *133* (23), 234303.

(57) Aguirre, N. F.; Díaz-Tendero, S.; Hervieux, P.-A.; Alcamí, M.; Martín, F. M3C: A Computational Approach To Describe Statistical Fragmentation of Excited Molecules and Clusters. *J. Chem. Theory Comput.* **2017**, *13*, 992–1009.

(58) Iyengar, S. S.; Schlegel, H. B.; Millam, J. M.; Voth, G. A.; Scuseria, G. E.; Frisch, M. J. Ab Initio Molecular Dynamics: Propagating the Density Matrix with Gaussian Orbitals. II. Generalizations Based on Mass-Weighting, Idempotency, Energy Conservation and Choice of Initial Conditions. *J. Chem. Phys.* **2001**, *115* (22), 10291–10302.

(59) Schlegel, H. B.; Millam, J. M.; Iyengar, S. S.; Voth, G. A.; Daniels, A. D.; Scuseria, G. E.; Frisch, M. J. Ab Initio Molecular Dynamics: Propagating the Density Matrix with Gaussian Orbitals. *J. Chem. Phys.* **2001**, *114* (22), 9758–9763.

(60) Schlegel, H. B.; Iyengar, S. S.; Li, X.; Millam, J. M.; Voth, G. A.; Scuseria, G. E.; Frisch, M. J. Ab Initio Molecular Dynamics: Propagating the Density Matrix with Gaussian Orbitals. III. Comparison with Born-Oppenheimer Dynamics. *J. Chem. Phys.* **2002**, *117* (19), 8694–8704.

(61) Gaussian 09, Revision D.01, Frisch, M. J.; Trucks, G. W.; Schlegel, H. B.; Scuseria, G. E.; Robb, M. A.; Cheeseman, J. R.; Scalmani, G.; Barone, V.; Petersson, G. A.; Nakatsuji, H.; Li, X.; Caricato, M.; Marenich, A. V.; Bloino, J.; Janesko, B. G.; Gomperts, R.; Mennucci, B.; Hratchian, H. P.; Ortiz, J. V.; Izmaylov, A. F.; Sonnenberg, J. L.; Williams-Young, D.; Ding, F.; Lipparini, F.; Egidi, F.; Goings, J.; Peng, B.; Petrone, A.; Henderson, T.; Ranasinghe, D.; Zakrzewski, V. G.; Gao, J.; Rega, N.; Zheng, G.; Liang, W.; Hada, M.; Ehara, M.; Toyota, K.; Fukuda, R.; Hasegawa, J.; Ishida, M.; Nakajima, T.; Honda, Y.; Kitao, O.; Nakai, H.; Vreven, T.; Throssell, K.; Montgomery, J. A., Jr.; Peralta, J. E.; Ogliaro, F.; Bearpark, M. J.; Heyd, J. J.; Brothers, E. N.; Kudin, K. N.; Staroverov, V. N.; Keith, T. A.; Kobayashi, R.; Normand, J.; Raghavachari, K.; Rendell, A. P.; Burant, J. C.; Iyengar, S. S.; Tomasi, J.; Cossi, M.; Millam, J. M.; Klene, M.; Adamo, C.; Cammi, R.; Ochterski, J. W.; Martin, R. L.; Morokuma, K.; Farkas, O.; Foresman, J. B.; Fox, D. J. Gaussian, Inc., Wallingford CT, 2016.

(62) Álvarez-Moreno, M.; De Graaf, C.; López, N.; Maseras, F.; Poblet, J. M.; Bo, C. Managing the Computational Chemistry Big Data Problem: The IoChem-BD Platform. *J. Chem. Inf. Model.* **2015**, *55* (1), 95–103.

(63) Sebbar, N.; Bozzelli, J. W.; Bockhorn, H. Enthalpy of Formation and Bond Energies on Unsaturated Oxygenated Hydrocarbons Using G3MP2B3 Calculation Methods. *Int. J. Chem. Kinet.* **2005**, *37* (10), 633–648.

(64) Vogelhuber, K. M.; Wren, S. W.; Sheps, L.; Lineberger, W. C. The C-H Bond Dissociation Energy of Furan: Photoelectron Spectroscopy of the Furanide Anion. *J. Chem. Phys.* **2011**, *134* (6).

AUTHOR INFORMATION

Corresponding Authors

* E-mail: marta.labuda@pg.edu.pl   ORCID: 0000-0003-0490-7294

* E-mail: manuel.alcami@uam.es   ORCID: 0000-0002-3753-5215

Author Contributions

The manuscript was written through contributions of all authors. All authors have given approval to the final version of the figures.
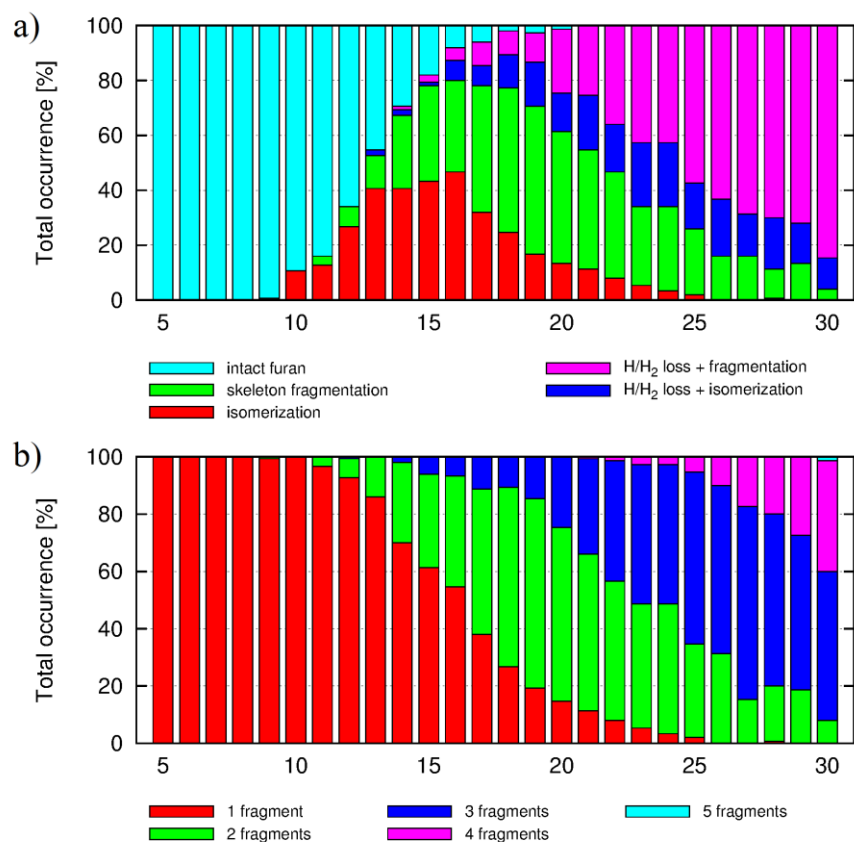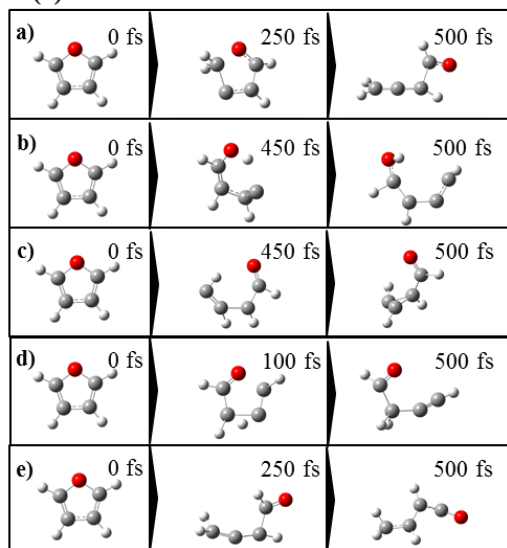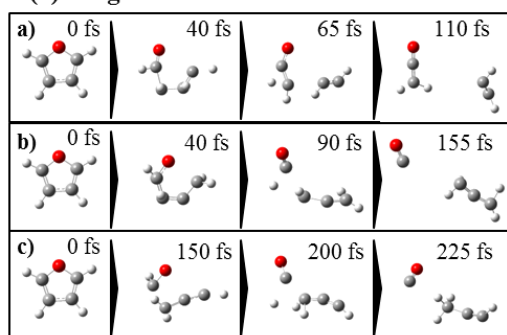
FIGURES

Figure 1 Results of ADMP simulations of neutral furan: Total occurrence of (a) the observed

processes and (b) the number of fragments as a function of the deposited energy.

(1) Isomerization

(2) Fragmentation

(3) H loss
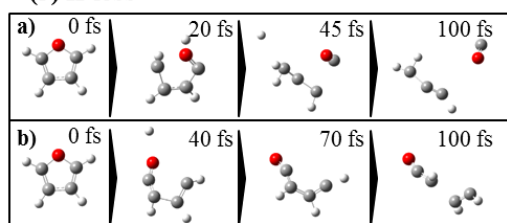
(4) H₂ loss
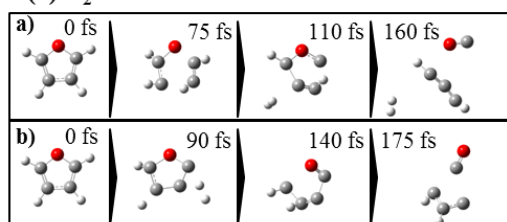
Figure 2 Snapshots of the most significant trajectories obtained in the ADMP simulations.
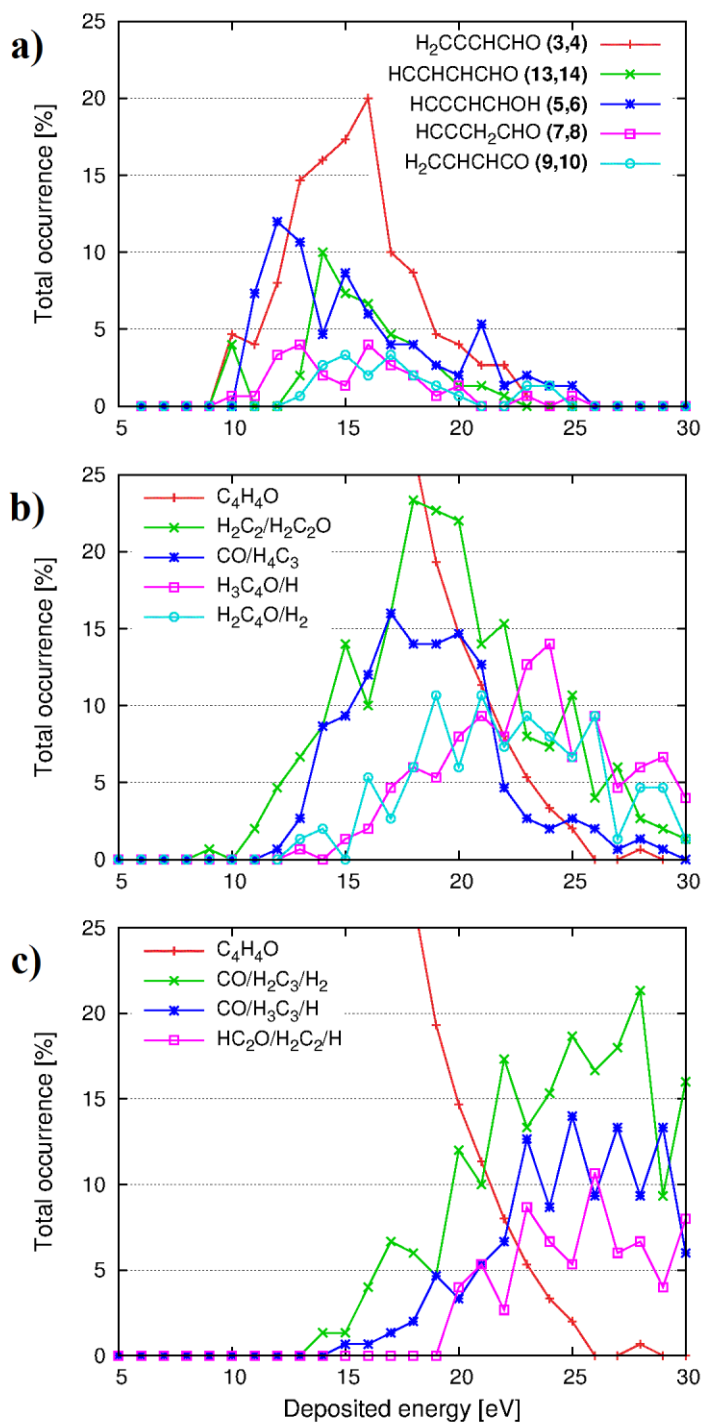
Figure 3 Results of ADMP simulations of neutral furan: (a) Isomerization (b) two- and (c) three-body fragmentation channels probabilities together with parent molecule as a function of the deposited energy.
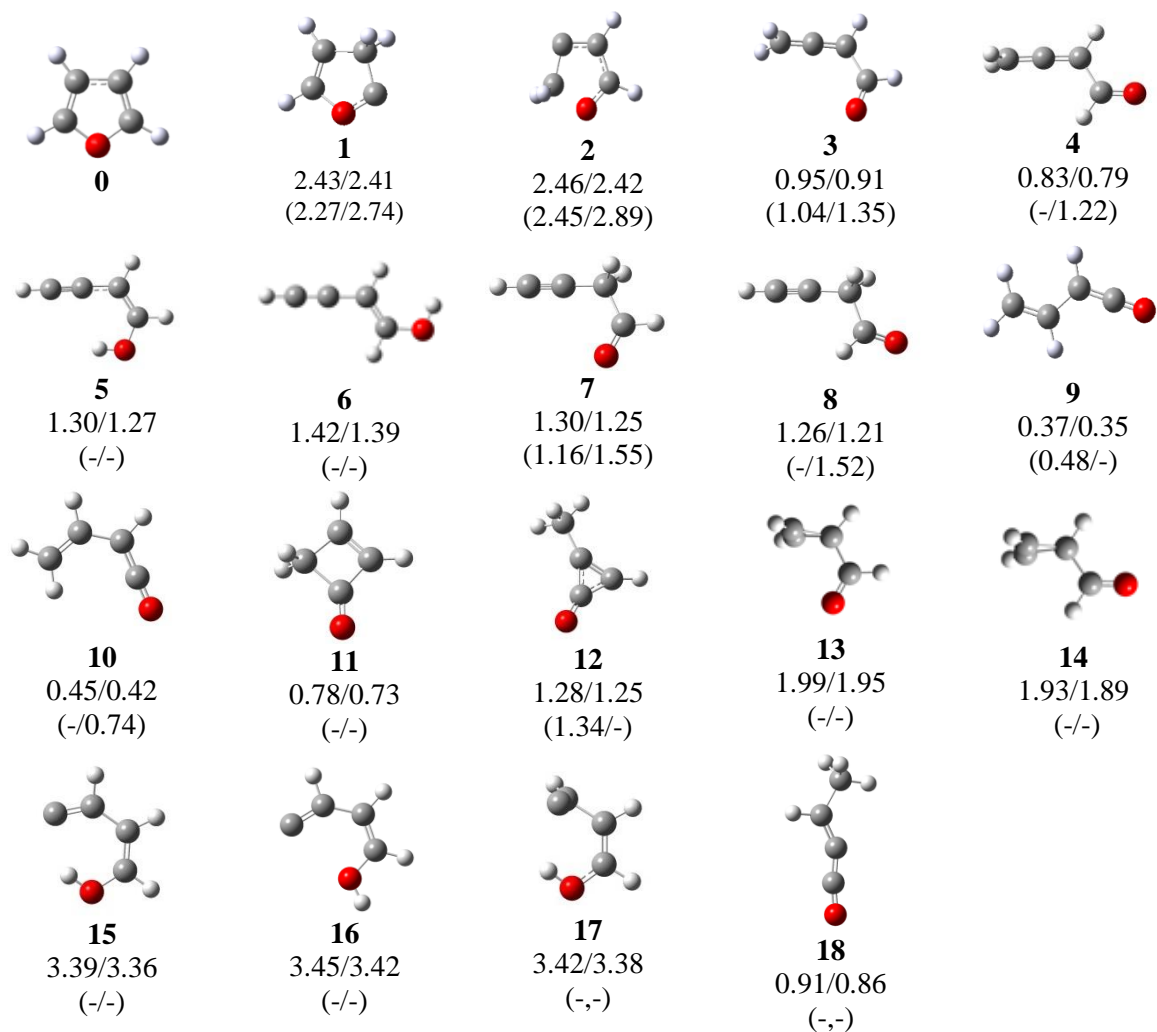
Figure 4. Structures obtained as minima of the PES for the isomerization of furan. Values of Relative Energies (in eV) with respect furan are given, first number correspond to the one evaluated at B3LYP/6-311++G(3df,2p), second value to the one evaluated at B3LYP/6-311++G(d,p) level. Comparison with previous calculations is given in parenthesis; first values are those reported by Liu *et al*. [47,48] and second ones those obtained by Sendt *et al*. [49]

33
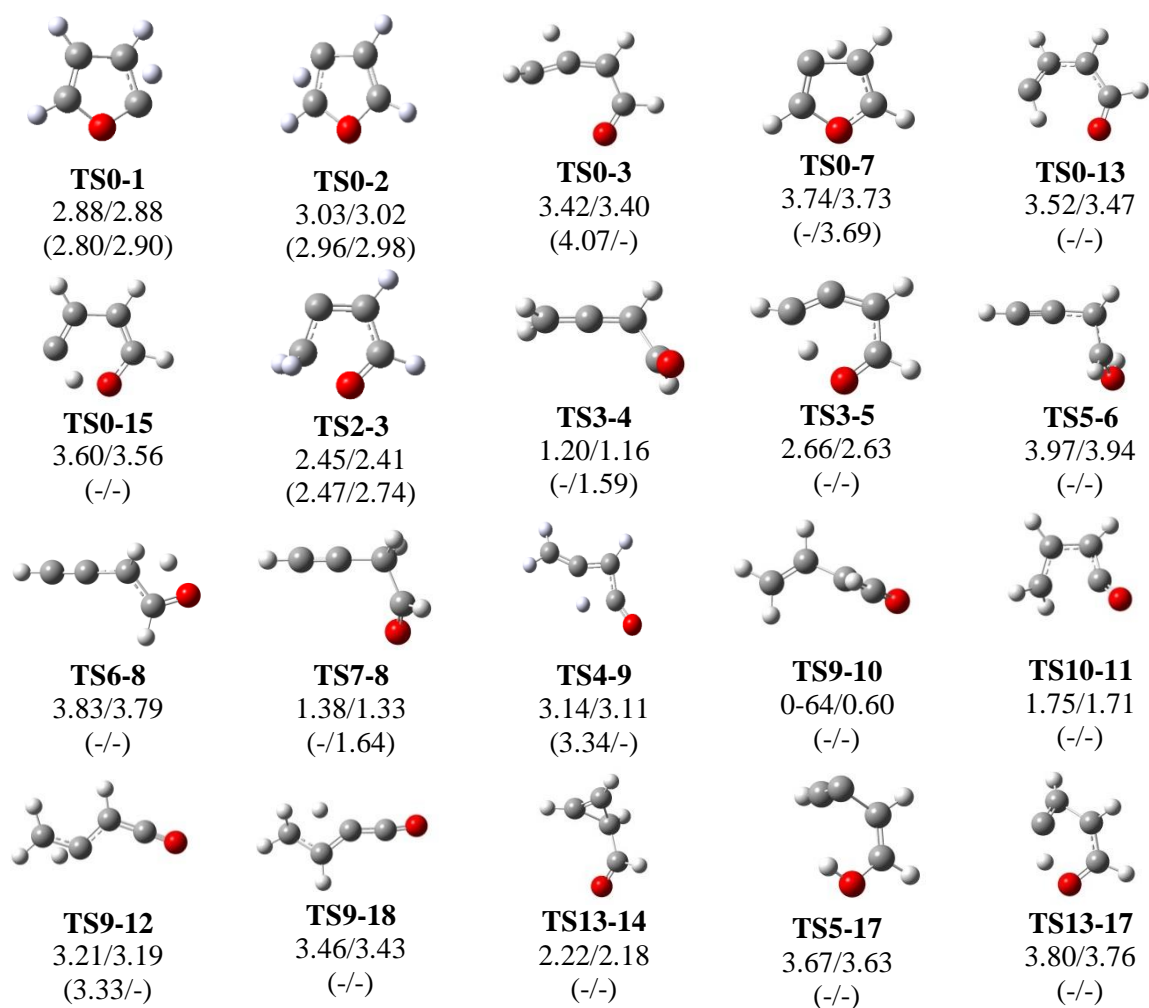
Figure 5 Structures obtained as Transition States of the PES for the isomerization of furan. Values of Relative Energies (in eV) with respect furan are given, first number correspond to the one evaluated at B3LYP/6-311++G(3df,2p), second value to the one evaluated at B3LYP/6-311++G(d,p) level. Comparison with previous calculations is given in parenthesis; first values are those reported by Liu *et al*. [47,48] and second ones those obtained by Sendt *et al.* [49]
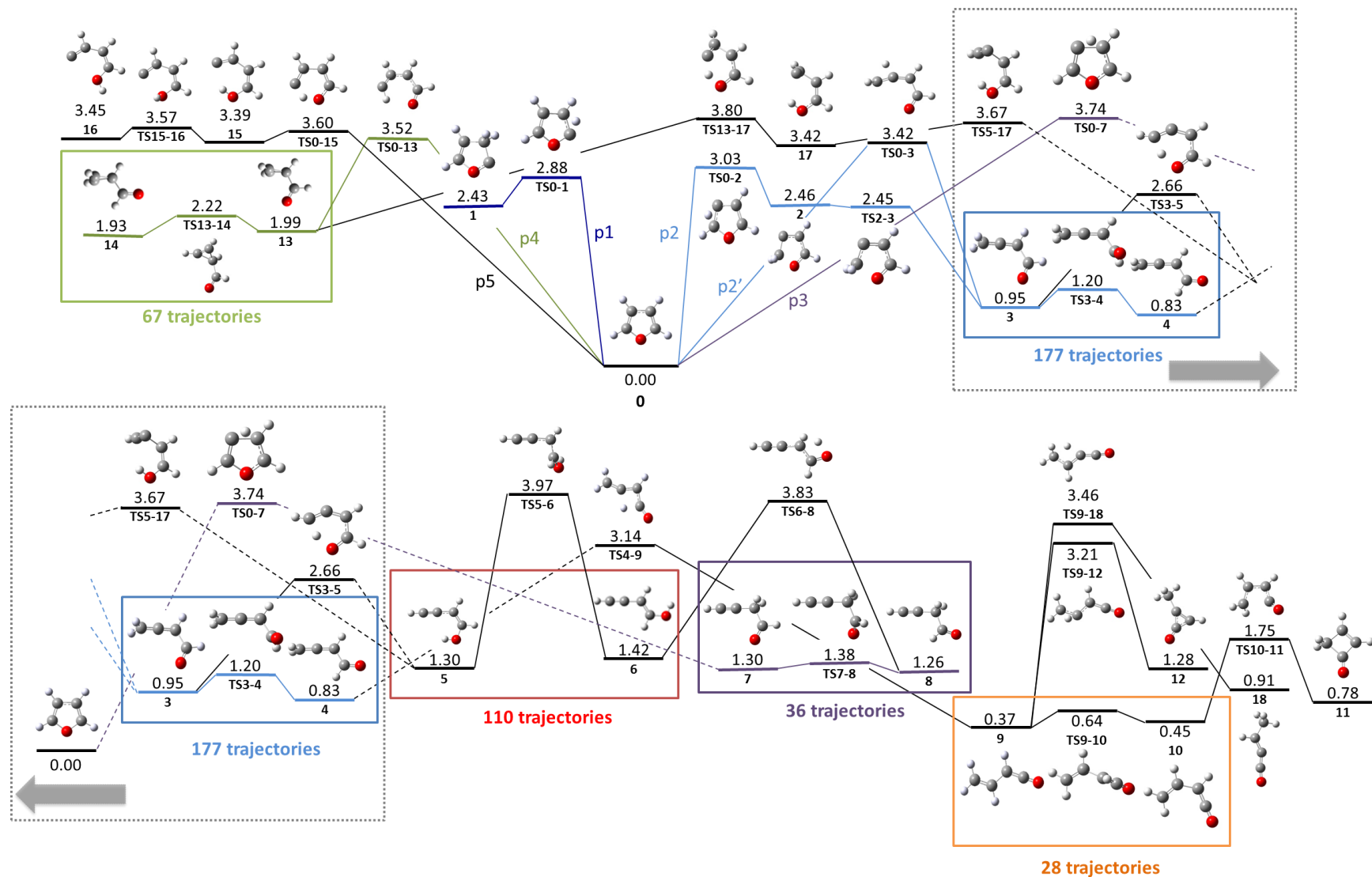
Figure 6 Diagram of the PES corresponding to isomerization processes. The reaction paths connecting all minima obtained in this work are given. The total number of trajectories, from all initial energies of the ADMP simulation, is indicated for each reaction pathway. Relative Energies with respect to furan (in eV) obtained at the B3LYP/6-311++G(3df,2p) level of theory are indicated for each structure and TS.
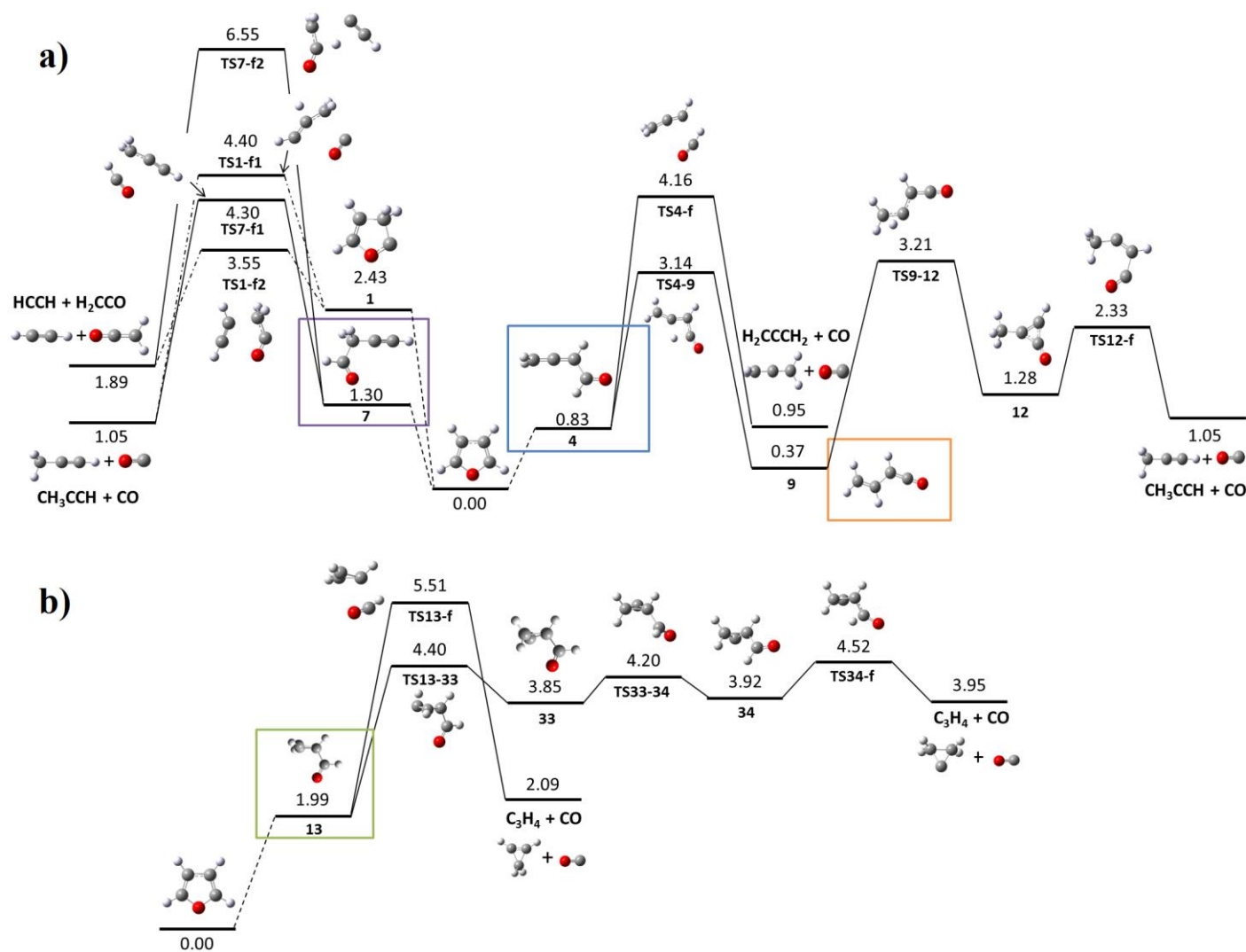
Figure 7 Skeleton fragmentation from the different isomers obtained in the present study. a) Fragmentation arising from isomerization pathways *p2* and *p3* of Figure 6. b) Fragmentation arising from isomerization pathways *p4*. For the sake of clarity some structures from Figure 4 have been also included. Relative Energies with respect to furan (in eV) obtained at the B3LYP/6-311++G(3df,2p) level of theory are indicated for each structure and TS.
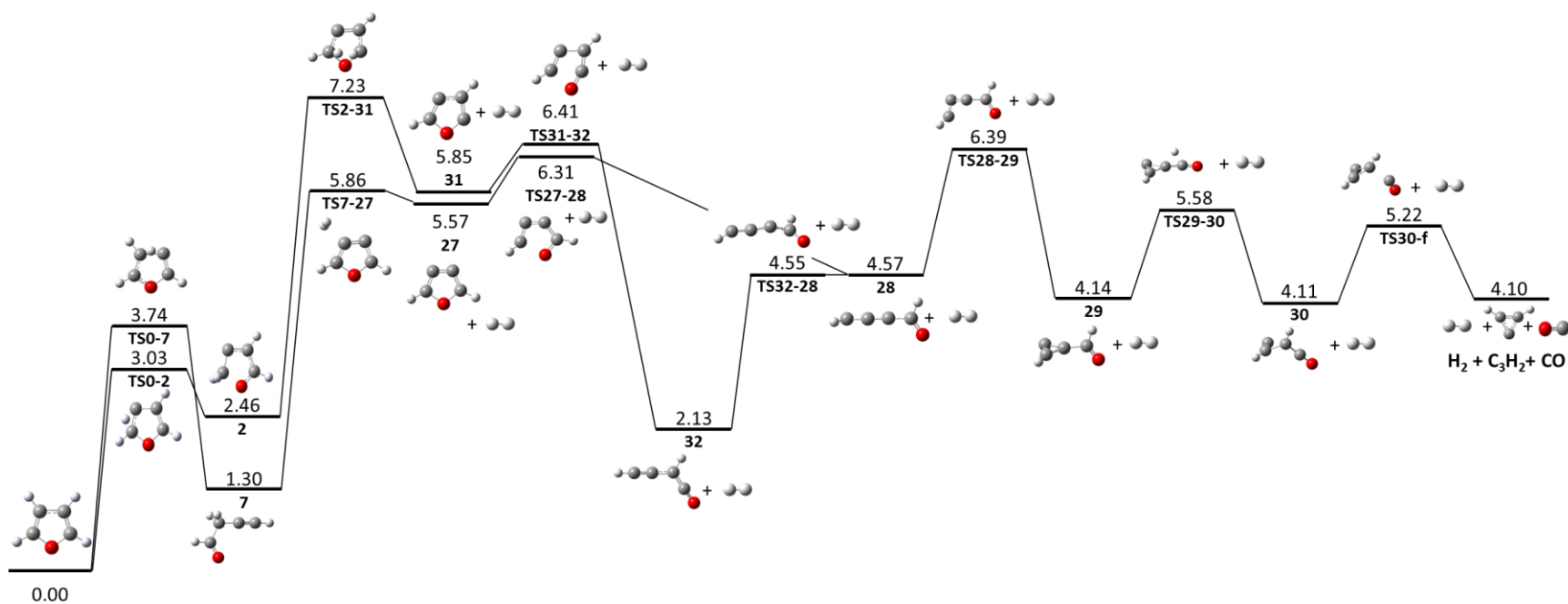
36
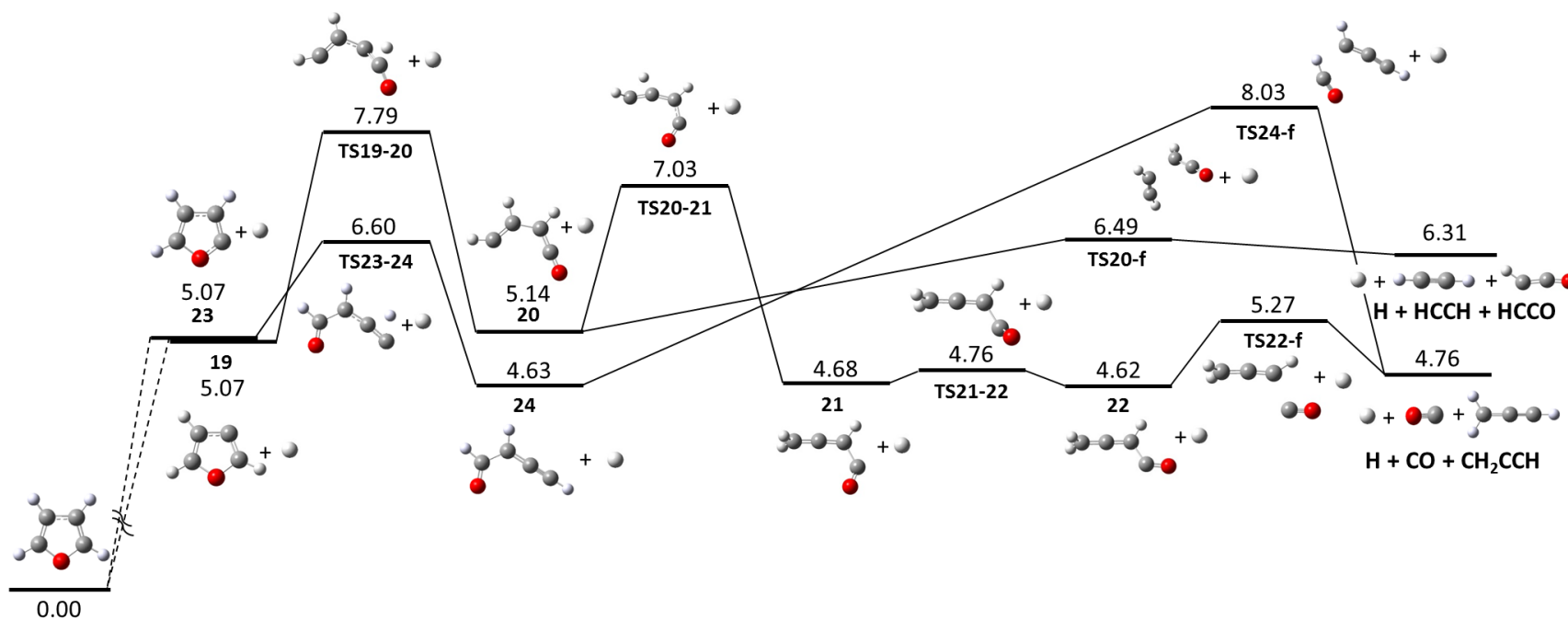
Figure 8 Fragmentation pathways after H loss process. Relative Energies with respect to furan (in eV) obtained at the B3LYP/6-311++G(3df,2p) level of theory are indicated for each structure and TS.

37

Figure 9 Fragmentation pathways after H_2 loss process from adjacent alpha and beta positions. Relative Energies with respect to furan (in eV) obtained at the B3LYP/6-311++G(3df,2p) level of theory are indicated for each structure and TS.
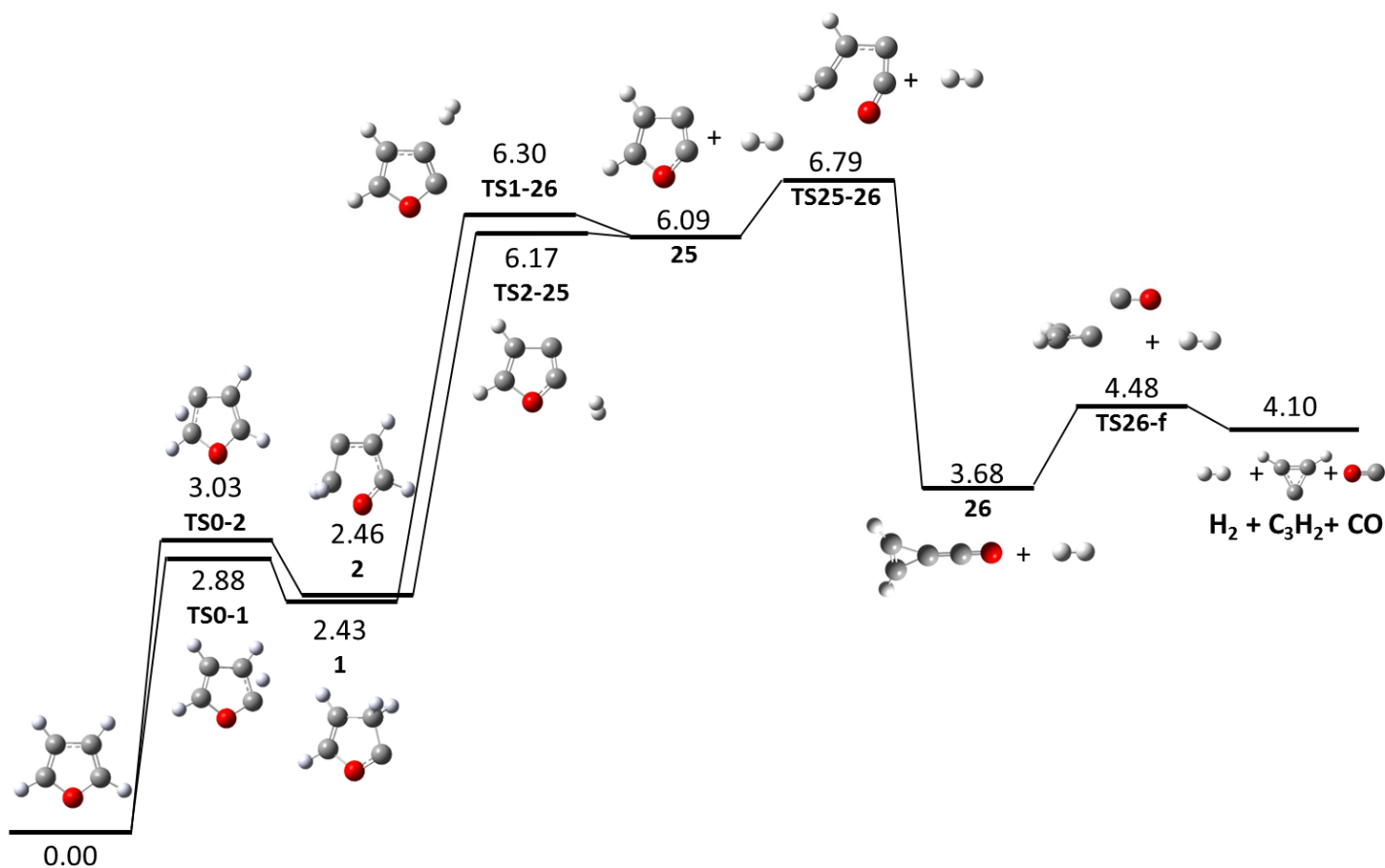
Figure 10 Fragmentation pathways after H_2 loss process from two beta positions, two alpha positions or opposite alpha and beta positions. Relative Energies with respect to furan (in eV) obtained at the B3LYP/6-311++G(3df,2p) level of theory are indicated for each structure and TS.
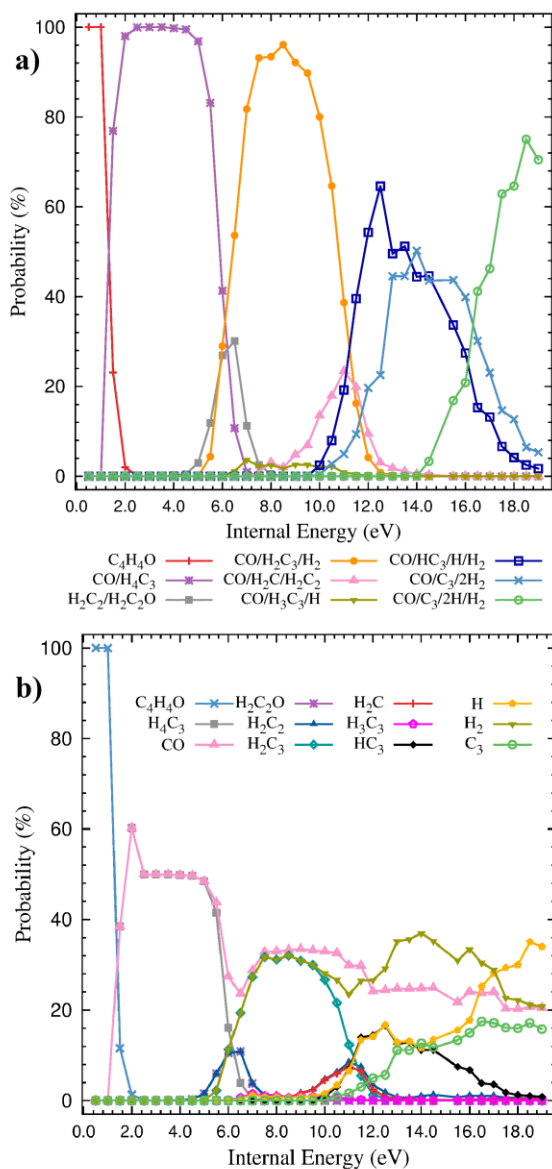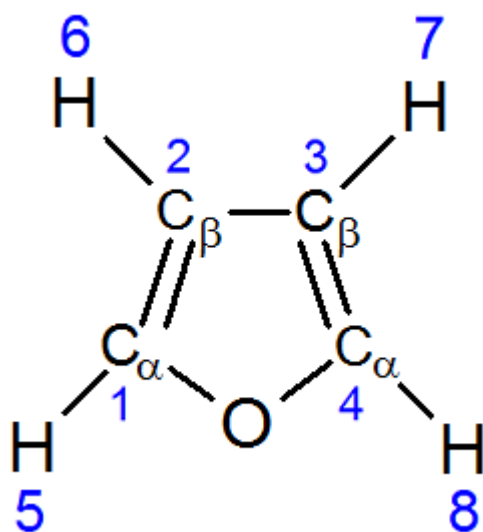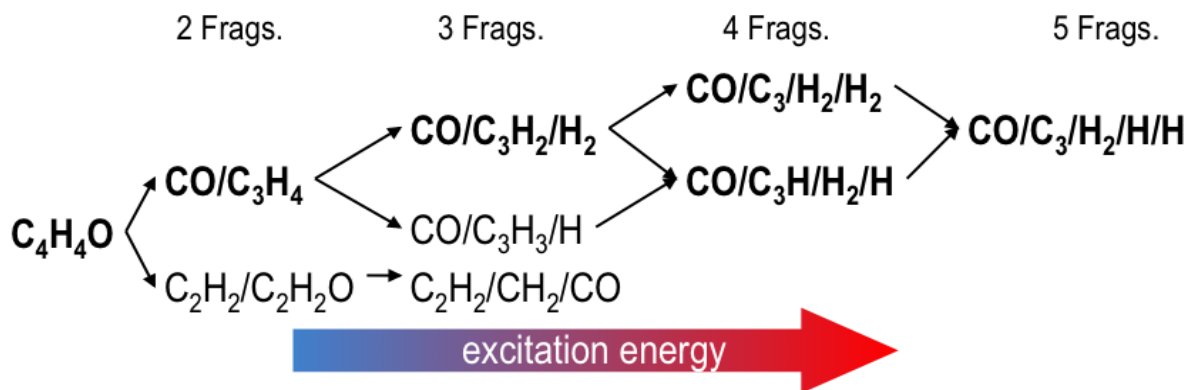
Figure 11 Fragmentation of the furan molecule from M$_3$C calculations: (a) Channels probability and (b) molecular species probabilities as a function of the internal energy of the system.

Scheme 1 Furan with the notation used for the identification of the different atoms.

Scheme 2 Observed channels in the M$_3$C simulations; the most probable ones are highlighted in bold.

TABLES

Table 1 Database of structures optimized at B3LYP/6-311++G(d,p) level of theory. The different electronic states are given and the numbers of isomers for each state is indicated in parentheses.

Atoms	Fragment	Isomer	Atoms	Fragment	Isomer
1	H	^2S	5	H_4C	$^1A_1$
	C	$^1D, ^3P$		H_3C_2	$^2A'', ^2A', ^4A_1, ^4A''$
	O	$^1D, ^3P$		H_3CO	$^2A', ^2A$
2	H_2	$^1\Sigma_g{}^+$		H_2C_3	$^1A_1(2), ^1A_g, ^1A, ^3\Sigma_g{}^+, ^3A''(2), ^3B_2, ^3A$
	HC	$^2\Pi, ^4\Sigma_g$		H_2C_2O	$^1A', ^1A_1, ^1A(2), ^3A''$
	HO	$^2\Pi$		HC_4	$^2A'(2), ^2A, ^2B_1, ^4A, ^4A''(4)$
	C_2	$^1\Sigma_g{}^+, ^3\Pi_u$		HC_3O	$^2A', ^4A$
	CO	$^1\Sigma_g, ^3\Pi$		C_4O	$^1A'(2), ^1A_1(2), ^3\Sigma_g$
3	H_2C	$^1A_1, ^3B_1, ^3A_2$	6	H_4C_2	$^1A, ^1A_g, ^3A'', ^3A_1$
	H_2O	$^1A_1$		H_4CO	$^1A'$
	HC_2	$^2\Sigma_g, ^2A_1, ^4A''$		H_3C_3	$^2B_1, ^2A', ^2A'', ^4A'', ^4A$
	HCO	$^2A'(2), ^4A''$		H_3C_2O	$^2A, ^4A(2)$
	C_3	$^1\Sigma_g{}^+, ^3A_1', ^3\Pi_g$		H_2C_4	$^1\Sigma_g, ^1A', ^1A_1(3), ^1A_g, ^1A, ^3A_2(3), A_u, ^3A(4)$
	C_2O	$^1\Sigma_g, ^1A_1, ^3\Sigma_g$		H_2C_3O	$^1A'(2), ^3A$
4	H_3C	$^2A_2''$		HC_4O	$^2A''$
	H_2C_2	$^1\Sigma_g, ^1A_1, ^3A_u, ^3B_2(2)$	7	H_4C_3	$^1A_1(3), ^1A(2), ^3A(2), ^3B_1, ^3A''(2)$
	H_2CO	$^1A_1(2), ^1A', ^3A''$		H_4C_2O	$^1A'(3), ^1A$
	HC_3	$^2A', ^2B_2, ^4\Sigma_g, ^4A''$		H_3C_4	$^2A''(2), ^2A(5), ^2A'(2), ^2B_2, ^4A_1, ^4A(4), ^4B_2, ^4A', ^4A''(6)$
	HC_2O	$^2A''(2), ^4A''(4), ^4A$		H_2C_4O	$^1A(2)$
	C_4	$^1\Sigma_g{}^+, ^1A_g, ^3\Sigma_g{}^+, ^3B_1, ^3A_1$	8	H_4C_4	$^1A'(6), ^1A(5), ^1A_1(2), ^1A_g(2), ^3A''(4), ^3A(8), ^3B_u, ^3A_g, ^3A_1, ^3A_2, ^3B_2$
	C_3O	$^1A', ^1\Sigma_g(2), ^3A'$		H_4C_3O	$^1A(3), ^3A$
				H_3C_4O	$^2A'', ^2A$
			9	H_4C_4O	$^1A'(16), ^1A_1(2), ^1A(3)$

$$S = k_B \ln \Omega(E)$$

Table of Contents Image